EFDA–JET–PR(12)34

K.K. Kirov, J. Mailloux, A. Ekedahl, V. Petrzilka, G. Arnoux, Yu. Baranov,
M. Brix, M. Goniche, S. Jachmich, M.-L. Mayoral, J. Ongena, F. Rimini,
M. Stamp and JET EFDA contributors

LHCD Operation with the ITER-Like Wall at JET

LHCD Operation with the ITER-Like Wall at JET

K.K. Kirov[1], J. Mailloux[1], A. Ekedahl[2], V. Petrzilka[3], G. Arnoux[1], Yu. Baranov[1], M. Brix[1], M. Goniche[2], S. Jachmich[4], M.-L. Mayoral[1], J. Ongena[4], F. Rimini[1], M. Stamp[1] and JET EFDA contributors*

JET-EFDA, Culham Science Centre, OX14 3DB, Abingdon, UK

[1]EURATOM-CCFE Fusion Association, Culham Science Centre, OX14 3DB, Abingdon, OXON, UK
[2]CEA, IRFM, F-13108 Saint Paul-Lez-Durance, France
[3]Association EURATOM-IPP.CR, Institute of Plasma Physics AS CR, Za Slovankou 3, 182 21 Praha 8, Czech Republic
[8]Association EURATOM-Belgian State, Koninklijke Militaire School - Ecole Royale Militaire, B-1000 Brussels Belgium
** See annex of F. Romanelli et al, "Overview of JET Results", (24th IAEA Fusion Energy Conference, San Diego, USA (2012)).*

Preprint of Paper to be submitted for publication in
Plasma Physics and Controlled Fusion

ABSTRACT

In this paper important aspects of Lower Hybrid Current Drive (LHCD) operation with the ITER Like Wall (ILW) [1] at JET are reported. Impurity release during LHCD operation was investigated and it was found that there is no significant *Be* increase with LHCD power. Concentration of *W* was analysed in more detail and it was concluded that LHCD contributes negligibly to its increase. No cases of *W* accumulation in LHCD-only heating experiments were observed so far. LHCD coupling was studied and optimised to achieve the level of system performance similar to before ILW installation. Measurements by Li-beam were used to study systematic dependencies of the SOL density on the gas injection rate from a dedicated gas introduction module and the LHCD power and launcher position. Experimental results are supported by modelling. Observations of arcs in front of the LHCD launcher and hotspots on magnetically connected sections of the vessel are reported. Overall, a relatively trouble-free operation of the LHCD system up to 2.5MW of coupled microwave power in L-mode plasma was achieved with no indication that the power cannot be increased further.

1. INTRODUCTION

ITER is designed to operate with beryllium (Be) main vessel and tungsten (W) divertor tiles due to the high fuel retention found on the carbon (C) based machines [2]. These are relatively new materials to be used as Plasma Facing Components (PFC) and little is known about the expected plasma performance of such all-metallic wall devices. The necessity of understanding the physics of plasma surface interaction and exploring the operational space for ITER initiated a project on installation of a new ITER Like Wall (ILW) at JET [1], [3]. The new JET wall has outboard Poloidal Limiters (PLs) and inner guard limiters made of Be, while the thermal load bearing divertor consists of W coated C tiles and bulk W tile assemblies.

After the installation of the ILW a number of key operational issues were addressed including: reinstating the robust plasma breakdown; being able to perform stable recovery pulses; and implementing protection of the new wall from plasma exhaust and energetic particles. In order to avoid melting the Be limiters, some restrictions on the heating power were necessary. Further, to reduce sputtering yield from divertor W tiles, JET needed to operate at lower SOL temperature, which was achieved by use of large gas puff rates and hence operation at higher density.

Although currently not planned, a Lower Hybrid Current Drive (LHCD) system is still under consideration for ITER [4], [5], [6]. While up-to-date experimental and theoretical studies are mainly focused on LH wave coupling and penetration issues and CD efficiency at ITER-like densities [7,8,9,10,11,12,13,14,15,16] no LHCD system has ever been tested at SOL conditions relevant to the PFC envisaged for ITER. Being equipped with LHCD system and ILW, JET provides a unique opportunity to study the performance of this Radio Frequency (RF) heating and current drive (CD) scheme in conditions as close as possible to ITER.

The use of the LHCD system at JET has been revised as a part of major review on the use of

all heating systems in conditions with the new wall. The power was limited initially to 180kW per klystron and 2.5MW of total coupled RF power. The position of the LHCD launcher, which can be controlled during JET pulse, was constrained within certain limits at high power operations. An attempt to improve the protection against arcs and to minimise their occurrence and/or avoid hotspots has been made. The latter are localised hot areas on PFC and can cause damage to the wall while the arcs can lead to plasma disruptions.

A new protection system named Protection of ITER-like Wall (PIW) [17], based on a set of new dedicated Infra Red (IR) and visible cameras and pyrometers, was introduced to monitor critical PFC and to prevent the PFC from reaching temperatures high enough to cause melting and damage to the wall. The upgrade of the monitoring systems included installation and operation of a new camera with a dedicated view of the LHCD launcher. The diagnostic features a shared view for IR imaging, visible camera and four pyrometers. The IR camera and the pyrometers were used to study hotspots and possible overheated areas in front of the launcher. The images from the visible camera were initially investigated to find out whether resolution and image quality are sufficiently satisfactory to use the camera to protect against arcs at the mouth of the launcher. After the first few pulses it was found that the visible camera image is too bright, especially when a large amount of gas is puffed from the dedicated gas introduction module situated near the launcher. Subsequently, a filter was installed in front of the camera which cuts all visible light above 550nm, thus reducing significantly the contribution from D_α signal. A later upgrade included installation of a filter which also filters out most intense Be lines thus further improving the quality of the image.
At the beginning of normal operation the focus of the JET program was more directed into issues related to fuel retention with the new wall, material studies regarding the new PFC, impurity accumulation and scenarios development. Priority was given to baseline and hybrid scenarios so LHCD was rarely used in the main program. As a result no LHCD pulses in H-mode were performed and results presented here are collected mainly from heating power conditioning sessions during the Restart period.

This paper gives an account on important aspects of the performance of the LHCD system with the ILW at JET for power levels up to 2.5MW and up to 5 seconds in duration. Initial observations were discussed in [18] and further developments are discussed below. A number of topics related to the new conditions associated with ILW are presented via comparison to the old C wall (CW). Throughout the paper the new data will be referred to as ILW conditions, new wall or new conditions while for the old C wall one of the following terms will be used: old conditions, old C wall or simply CW. If not explicitly noted in the text one should assume that all JET pulses prior to pulse number 79854 are in conditions with CW, whilst newer pulses are with ILW. The discussions addressed here are split into three major topics: (i) impurity release during LHCD operation; (ii) coupling issues in conditions with the new wall and (iii) observations and analysis of arcs and hotspots. Section 2 gives an account of the important changes to the LHCD system with installation of ILW. Section 3 discusses observations of impurities related to LHCD and ILW.

Section 4 is dedicated to coupling studies and it also provides important results on SOL density measurements and modelling. Observations of arcs and hotspots are discussed in Section 5. The last Section is dedicated to conclusions and remarks regarding future operation of the system and on-going projects aiming at improvement of the arc detection system.

2. LHCD SYSTEM AT JET

The LHCD system at JET is detailed in [19], [20] and more details, including a number of recent restrictions imposed on LHCD operations, are discussed in [21]. Here only an account of the system components which have been affected by the ILW installation will be given.

The LHCD launcher at JET has an active radiating part, so called multijunctions [22] or sometimes for simplicity called the "grill". It consists of open-ended waveguides arranged in a phased-array antenna structure. It is fed by 24 klystrons grouped in six modules, each pair of which can power two separate rows. The multijunctions are bound by a passive structure, referred to as a frame, which protrudes about 0.003m to 0.005m in front of the grill thus protecting it from interaction with hot plasma and energetic particles. A picture of the launcher front end, or so called mouth, with notations of the six rows and the launcher surroundings is shown in figure 1. Reflection Coefficients (RCs) are measured as a ratio of the reflected to the forward RF power averaged along each row, RC1 to RC6 for rows 1 to 6, and good coupling is defined to be RC≤0.08. If the electron density in front of the launcher is not sufficiently high the coupling of the RF wave deteriorates as a large amount of the RF power is reflected back to the waveguides and so the RCs increase. The risk of developing arcs and causing damage to the launcher in this case is very high. At JET there are a couple of ways to improve the coupling when the density in front of launcher is not sufficiently high. The first method is to move the launcher closer to the denser plasma and the second is to use gas injection from the dedicated gas introduction module situated near the LHCD launcher, figure 1b. Two limiters are situated on each side of the launcher; the one on the left is normal Poloidal Limiter (PL) while the right-hand one is narrower PL (nPL). The smaller width of the nPL restricts its load bearing capacity so it is aligned 0.005m behind the normal PLs. The distance between the LH launcher and plasma is measured by two quantities: launcher to nPL distance, l_{pos}, and separatrix to PL clearance at midplane, r_{ROG}. Negative values of l_{pos} mean the launcher is behind the nPL hence the real distance between the separatrix and launcher at midplane is the sum $r_{ROG}+0.005-l_{pos}$. More details on the geometry are provided in [21].

During the Shutdown in 2010 a couple of modifications were made to the launcher. While all the sections of the old frame were made of C or CFC, figure 1a, the new tiles were manufactured from Be, figure 1b, in order to comply with the requirement for an all-Be PFC. The grill is made of stainless steel and this has not been changed. Although the new frame looks different from the old one, especially the corner sections, the geometry of the sides was kept essentially unchanged. The same applies for all the limiters surrounding the launcher meaning that, from the geometrical point of view, the scrape-off lengths are the same as with the old wall. The dedicated gas introduction

module, figure 1b, is about 1m on the left of the launcher and has not been changed.

During the ILW Shutdown two other important changes to the launcher were made. After a photographic inspection of the grill it was decided to undertake an intervention, which aimed at removing the most severe droplets and blobs due to melting of the grill. These were deemed to be potentially dangerous regarding arcing at the grill. This kind of work has been done before in the previous shutdowns without seeing any effect on the LHCD coupling and plasma-launcher interactions.

The other change related to the launcher was with respect to its position. A photogrammetric measurement was used to revise the launcher position and it was found that the launcher is about 0.019m in front of what was measured in the previous campaigns. It is not clear when this discrepancy happened but it is believed that this offset was present in the previous few campaigns before the Shutdown in 2010. Subsequently the launcher position, l_{pos}, was corrected in accordance with the new findings, and all data in this paper uses the position based on the revised measurements.

3. IMPURITIES RELATED TO ILW

An impurity release during LHCD operation was investigated using the spectral intensity of Be line normalized to the line integrated density to provide a database covering all LHCD-only pulses at JET with ILW.

The intensity of the BeII line (single stage ionised Be) at 527nm is observed predominantly at the edge as typical plasma parameters of the L-mode periphery were $n_e(\psi_N = 0.9) \approx 1.7\times10^{19} m^{-3}$ and $T_e(\psi_N = 0.9) \approx 170eV$, where ψ_N is the normalised poloidal flux. Data was collected and averaged over steady-state time intervals during LHCD conditioning pulses. The essential plasma parameters (configuration, density, temperature and fuelling rate) in the LHCD database do not vary significantly, while the processes involved in impurity generation and transport are not accounted for. The line emission intensities are then normalised to the line integrated density during LHCD, $I_{BeII}/n_e(LH)$, and for a non LHCD reference, $I_{BeII}/n_e(noLH)$, which is taken shortly before the system is turned on. The average values for all LHCD-only pulses are $I_{BeII}/n_e(LH) \approx 5.0\times10^{-8}$ (p/s cm^2 sr m^{-2}) and I_{BeII}/n_e (noLH) $\approx 5.7\times10^{-8}$ (p/s cm^2 sr m^{-2}) showing small, slightly negative changes of the emission during LHCD. The changes of the normalized emission is calculated as $\Delta(I_{BeII}/n_e) = I_{BeII}/n_e(LH) - I_{BeII}/n_e(noLH)$ and is studied versus the coupled LHCD power. The results in figures 2a are, therefore, interpreted as an estimate of the increase of the Be density at the edge due to LHCD heating power.

It was found that for up to 2.5MW there is no consistent increase in Be in LHCD-only experiments, figure 2a. The data is relatively scattered; however, statistically averaged figures also show no trends of normalised BeII line radiation with LHCD power.

The concentration of W is studied in more detail using a dedicated analysis code [23], which collects data from available spectrometers and bolometers and uses plasma profiles from various diagnostics to assess the concentration of W assuming that the intensity of the spectral lines emitted

by highly ionised W atoms depends mainly on the fractional abundance of the emitting ionisation stage. The ionisation equilibrium is evaluated according to the findings in [23], [24], where it has been shown that the transport can be neglected. The photon emissivity coefficient is evaluated for electron impact excitation in the framework of collisional radiative model.

For typical LHCD conditioning pulses it was found that the average W concentration, $C_{w,LH}$, in the core at about one third of the normalised minor radius was of the order of 5×10^{-6}. It drops to about $C_{w,OH}$ 4×10^{-6} after the LHCD power is turned off during Ohmic (OH) only heating. These values are relatively low assuming the detection limit of the model is of the order of 1×10^{-6} to 2×10^{-6}. Evaluating the errors in this assessment is difficult due to the large number of diagnostics involved and assumptions in the model. The reported [25] values for ICRH and NBI only heating are at least of order of a magnitude higher for power levels of 2.5MW and higher. It should be noted, however, that this evaluation is not meant for comparison between different heating powers but instead is provided to illustrate the typical range of change of C_w with auxiliary power. The latter also depends in a complex way on many parameters as for instance: the type of additional heating, the power deposition profiles, plasma configuration, fuelling and a number of plasma and SOL parameters. The contribution of all these factors is not investigated in this paper as their variation during LHCD conditioning pulses is relatively small.

The increase in W concentration, $\Delta C_w = (C_{w,LH}-C_{w,OH})/C_{w,OH}$, during LHCD is shown in figure 2b. Relative changes are calculated after averaging over the LHCD phase and using an OH time slice before or after LHCD for a reference. Although data is insufficient to draw a firm conclusion, for LH power in the range 1–1.5MW there is small, about $\Delta C_w \approx 25–30\%$, increase in W concentration. This value slightly increases with increasing the power above 2MW reaching about $\Delta C_w \approx 40–50\%$ but in this dataset the absolute W concentration never exceeds 1×10^{-5}. Moreover, in all the cases shown here the LH was pulsed with gas injection from a dedicated gas valve, which itself might have an impact on the SOL conditions and particularly SOL temperature and sputtering yields and hence on impurities. For instance, the negative point in figure 2b can be interpreted as an indication of reduction in C_W due to impact of the increased gas injection rate shortly before LHCD is applied. In order to provide good coupling, LHCD was always pulsed with gas from the dedicated gas injection module, so the LHCD power and increased gas introduction rate cannot be separated as contributors in the analysis. Time traces of an LHCD conditioning pulse with magnetic field, plasma current, density, gas puff rate and an estimate of C_W levels for the largest ΔC_w case are shown in figure 2c. It should be noted that during LHCD the concentration of W is of the same order as during low-power (1MW) NBI heating and C_W definitely does not increase more than twice compared to OH phase.

Tungsten accumulation during LHCD is also analysed by means of a bolometric diagnostic, which provides the total radiated power and radiation from the core only. In the case of W accumulation, core radiated power becomes dominant and correlated with increased line emission of highly ionised W ion stages detected by the available VUV spectrometers. The total and the

core-only radiated powers are taken at the beginning and at the end of all LHCD-only pulses and analysed consistently with the data from spectrometers in order to assess impurity accumulation with LHCD. The analysis has shown that no persistent W accumulation event has been detected during LHCD-only pulses. The cases in which the core radiated power becomes dominant were analysed and it was found that this is either due to events associated with arcs and related Fe influx or, in a few cases, a sudden increase in W line radiation is observed. However, in all cases of W influx the impurity radiation is of transient nature and it quickly (hundreds of ms) recovers to normal levels registered before the event has taken place.

4. COUPLING STUDIES

During the initial phase of JET Restart after completing ILW installation the main focus of the LHCD system was bringing up the power to a milestone of 2.5MW. For this purpose, repetitive pulses in similar conditions and configurations were executed as the power was increased gradually. The launcher position was restricted at high power, i.e. l_{pos}>-0.015m for klystron power larger than 180kW, as a precaution regarding melting the limiter tiles if the magnetic field lines become too incident to the tiles' surface. To allow controlled tests at high instantaneous LH power, modulated power waveforms were used at the beginning, with the amplitude increased or the modulation depth decreased after a number of successful pulses. Plasma configuration, total gas injection and plasma density were not varied significantly. As the goal of these sessions was merely to increase the power up to a set milestone rather than studying the LH coupling under various conditions, the only two adjustable parameters available were the gas rate from dedicated gas injection valve and launcher position.

4.1 LHCD COUPLING IN CONDITIONS WITH THE NEW WALL.

Two main factors were expected to have a significant effect on the LHCD coupling with the ILW, compared to the old wall conditions. Due to the new metallic wall one would expect different recycling and impurities thus different SOL conditions. Also, in order to decrease the SOL temperature, thus reducing the sputtering yield, all operations with the ILW at JET used large gas puff rates. These issues were expected to have an impact on the LHCD performance so time was dedicated to studying their contributions in the new conditions of ILW.

Changes to the LHCD coupling conditions during conditioning experiments with ILW will be discussed and discrepancies between ILW and CW will be highlighted. Most of LHCD conditioning pulses were in L-mode either at 2.2T or 2.4T, while the plasma current was 2MA. The plasma density was in general relatively high with line averaged values between 2.3 and 2.5×10^{19} m^{-3}. In conditions with CW the line averaged plasma density during LHCD conditioning was of the order of 2.0×10^{19} m^{-3}, i.e. somewhat 20% smaller. An example of typical LHCD conditioning pulses in old conditions and with ILW is shown in figure 3.

Time traces of the two pulses (figure 3a) clearly show the differences in density and gas injection

rates; total and from a dedicated gas valve. JET uses a set of predefined plasma configurations, figure 3b, exclusively developed for conditioning purposes and for LHCD the configuration being used is optimized to provide good coupling conditions with the outer strike point on the horizontal tile of the divertor. Although the configurations being used with CW and during ILW Restart are very similar (figure 3b) the distances between the launcher and the limiter were slightly larger during the ILW experiments (figure 3a shows the ILW r_{ROG} around 0.05m compared to r_{ROG} ≈0.04m with CW). There are further differences between launcher-plasma clearance as with ILW most of the pulses were at either l_{pos} ≈0m or -0.005m while with CW a value for l_{pos} between +0.009m and -0.006m was usually selected. Although the electron density in the new pulses was larger (figure 3c) an extra gas puff of about 4×10^{21} el/s from dedicated gas injection valve was now needed to provide good coupling. Despite obvious differences, the RCs, averaged over rows 1 to 6, in conditions with ILW are relatively low (figure 3a) indicating that in general LH wave coupling was not significantly degraded by the new wall. The large sudden changes of RCs in ILW case (figure 3a bottom) is due to sudden tripping of a klystron by the protection system. Close examination shows that when the tripping kystron is re-energised the reflected power suddenly increases leading to an imbalace which further trips the klystron, hence the ragged form of RC.

A more detailed comparison of the coupling conditions was carried out after cross-checking the averaged RCs for pulses in which SOL conditions and plasma parameters are similar. In order to find a suitable set of pulses to compare, early ILW plasma commissioning pulses in lower density regime were checked.

In figure 4 an example with similar electron density (figure 4c) total gas injection, configuration (figure 4b) and plasma-launcher distance are shown. Dedicated gas injection valve was not used in these two pulses. After comparing the coupling on individual rows (figure 4a bottom graph) it was found that the RCs on the top and at the middle of the launcher are approximately the same confirming the conclusion that for this part of the grill coupling is not affected for the selected examples. The bottom two rows, RC5&6, however, measure higher RCs with ILW compared to CW. Adding gas puff from a dedicated gas valve, a well known remedy to lower the RCs [26,27,28,29], improves the coupling on the bottom rows. It is unclear whether in different conditions, e.g. lower density or different configuration and plasma-launcher distance, this conclusion will still hold. A comprehensive analysis would require similar comparison for the whole range of plasma conditions in which LH is used.

4.2 SCAN OF GAS INJECTION RATES FROM DEDICATED GAS VALVE.

In the process of optimising the LH system performance, the gas injection rates were scanned and it was found that coupling improves on all rows with gas injection rate. An example is shown in figure 5a, where RCs of rows 1 to 6, RC1 to RC6, are shown for four different values of the gas injection rates, namely 0, 2×10^{21}, 4×10^{21}, 6×10^{21} el/s. Power waveforms, gas puff rates and line-integrated electron density are also shown in figure 5b. For the middle rows, 3&4, with RC3 and RC4, the

coupling is good, RCs<0.08, even without gas. Higher rates of injection further reduce the RCs on these rows. The top two rows, 1&2, need rates of about 4×10^{21}el/s to achieve a reasonable coupling and to stop being tripped by the protection system, based on the imbalance in the reflected RF power. In contrast, the bottom rows, 5&6, show bad coupling, RCs>0.12, for lower gas rates and good coupling is only achieved at maximum gas injection rate used in the experiments, 6×10^{21}el/s.

4.3 SOL DENSITY MEASUREMENTS

The JET Li-beam diagnostic was substantially upgraded [30] during ILW installation work. Measurements were used to assess the Scrape-off Layer (SOL) density modifications due to LHCD. For plasmas with 2.7T/2.45MA or 2.2T/2MA the middle of the LHCD grill, i.e. rows 3&4, is magnetically connected to the diagnostic, while the top, rows 1&2, and the bottom of the launcher, rows 5&6, are not connected. For the gas scan pulses discussed in the previous Section, Li-beam measurements were performed and time traces of the power waveforms, gas puff rates, line integrated, central, pedestal and SOL densities are shown in figure 5b. The bottom graph provides the density in front of the PL with a midplane position of about R_{mid} ≈3.889m, which is about 0.04m outside the separatrix. Density profiles for Pulse No: 81299 with gas rate from dedicated valve of 4×10^{21}el/s at different time slices are also shown in figure 6a.

For the time slice at 9.85s magnetically connected rows 3&4 were pulsed and density increases between R_{mid} ≈3.87m and 3.89m. At 10.09s, heating was turned off while at 10.85s and 11.09s the top, 1&2, and the bottom, 5&6, rows were pulsed respectively. As these parts of the grill are not connected to the Li beam diagnostic, the density stays unchanged. The observed effects are poloidally inhomogeneous and separated in a sense that only the flux tube in front of the powered sections of the grill show changes in density as it can be seen from time traces at the bottom of figure 5b as well. From the time traces in figure 5b and the profiles in figure 6a it is clear that the LHCD power modifies the SOL density profile in front of the powered sections of the launcher only. The modifications are local, i.e. when rows 1&2 are energised no changes to SOL density in the flux tube connected to rows 3&4 is seen as the time traces at the bottom of figure 5b remain flat in time intervals 11s-12s and 12s-13s. At a maximum gas injection rate row 5&6 can also affect the density in front of rows 3&4. As a result of these changes to the SOL density the LH wave coupling is improved, also shown by RCs trends in figure 5a. Individual profiles with rows 3&4 powered at 9.5s and no LH power at 10.5s for different rates of gas injection are shown in figure 6b. It was found that the increase in SOL density is 'hump' shaped and scales with gas injection rate. An interesting observation is that even without gas from a dedicated gas injection valve, the LH power affects the SOL density, as shown by the green profiles in figure 6b.

In addition, SOL density changes were studied as a function of LH power and launcher position. The SOL density increases with increasing the coupled RF power, figure 6c. In this example LHCD power was ramped-up (figure 6c inset graph) while the plasma parameters and the configuration were not changed indicating that processes involved are acting on a very fast time scale. The changes

of SOL density were more dramatic when the power was increased from 0.42MW to 0.87MW and very small for changes from 1.56MW to 2.02MW. This suggests that the process which takes place in front of the launcher has a threshold and possibly saturates at higher power levels. The behaviour of local density changes while retracting the launcher backward is shown in figure 6d, e. It can be concluded that the hump is moving with the launcher thus forming a big dip region when the latter is at its farthest position.

4.4 EDGE2D MODELLING

Local density modifications, and in particular the appearance of a hump in front of the launcher, have been observed and successfully modelled [31] with the two dimensional code EDGE2D [32] in the old JET conditions. This modelling did not include LH power, which causes a strong enhancement of the hump (figure 6). The code has therefore been modified to take into account the presence of limiters in the SOL and the heating in the SOL by a fraction of the LHCD power and newer simulations, which include LH power losses in the SOL are reported in [33] as well. The heating in the SOL is thought [33] to contribute to the density increase, either because of the SOL heating by collisional dissipation of the LH wave or due to the fast electrons parasitically created by the LH wave in front of the grill mouth [34], or both. The model cannot predict precisely the $N_{||}$ spectrum of the parasitically absorbed RF power. Results of the simulations are shown in figure 7.

The model can predict reasonably well the changes in SOL density profiles with LH power figure 7a, gas injection rate, figure 7a and b, and launcher position, figure 7c. In the case when no gas from dedicated valve was used the code was first tested and found in good agreement with measurements for $P_{LH} = 0$ (see blue lines in figure 7a). The changes in SOL profile with LHCD power were best simulated assuming about 10kW of LHCD power absorbed in the SOL (magenta lines in figure 7a). The calculations are more consistent with the experimental results in the cases when gas from dedicated valve was used; however, in the simulations about twice smaller gas puff rate was needed to reproduce the changes in SOL density with LHCD power (see figure 7b). An increase in dissipated power was needed in order to reproduce the density changes when launcher is moved forward in front of the limiter (figure 7c). On-going modelling activity aims at explaining the observed results and dependencies. For the purpose of the paper, however, it is important to note that the observed density changes can be reproduced assuming small amount of RF power is absorbed in the SOL.

From these simulations it can be concluded that only a few percent (maximum of about 5–6%) of the launched power is absorbed by the SOL plasma in the magnetic flux tubes in front of the LHCD grill. The power dissipation heats the electron fluid, which results in the ionization of the neutral gas. The gas was injected in simulations from poloidal locations corresponding to the dedicated gas injection valve location. The gas was ionized due to its interaction with the SOL plasma, which was heated by the parasitic absorption of the LH wave in the SOL. The power dissipated in the SOL needed for the fit of the modelling to the Li-beam measurements is indicated in figures.

5. ARCS AND HOTSPOTS

Issues related to possible harmful interaction between LHCD and plasma, in particular in the SOL region, were monitored via the available viewing systems. In addition to the new cameras used for protecting first wall components of JET, dedicated diagnostics have been installed to protect against, and study, the parasitic loss of LH power in the SOL (respectively, pyrometers viewing the LH launcher and the nearest poloidal limiter, and a dedicated infrared (IR) camera). An unfolded view of JET interior showing camera views is provided in figure 8. Projections of magnetic field lines covering the LHCD launcher boundaries from top to bottom in a typical 2.4T/2MA conditioning pulse are provided as well. Shown are the views of the cameras used in the study, namely, LHCD camera, wide angle IR and divertor camera. LHCD camera has visible CCD and IR imaging system. The approximate positions of the hotspots discussed in the study are indicated as well.

Arcs in front of the LH grill can be monitored by the visible LHCD camera, figure 8, while hot spots can be seen by IR camera. Examples of hotspot observation presented here are on (1) the ICRH ITER Like Antenna (ILA) antenna left side limiter seen by wide angle IR camera; (2) on horizontal tile of the outer divertor and (3) on the top of divertor apron as seen by the divertor camera. All these places are indicated by arrows in figure 8.

5.1 OBSERVATION OF ARCS VIA A DEDICATED VISIBLE CAMERA

Amongst the number of protection issues which were addressed during the LHCD operation with ILW at JET, arcs were thought to be potentially the most dangerous events. Arcing is dangerous not only because it causes damage to the launcher but also due to the associated large impurity influx of Fe, which sometimes causes plasma disruption. Arcs are now monitored by a new dedicated visible camera, figure 8, viewing the whole LH grill with sufficient resolution to identify on which part of the LH grill the arc is taking place. The implementation of the camera though was not straightforward; initially it was found that the ambient light in front of the launcher brightened the image and did not allow adequate visibility. A number of filters were tried while the contrast was optimised. The goal was to filter out the ambient light, i.e. bremsstrahlung and line emission due to different collisional processes taking place in the SOL, while still being able to detect light coming from an arc, and this was achieved.

For the first time at JET the dynamics of arc development have been observed (figure 9). It has been seen that if a localised arc is not extinguished fast enough by the existing protection systems, (based on the reflected power imbalance and on the impurity radiation) it can propagate along the grill mouth thus covering a much broader area, which might result in substantial damage to the launcher. After successfully implementing the new viewing system, 16 arcing cases were detected out of total 231 conditioning pulses. It was also observed that some arcs were stopped by the protection systems but some were not extinguished in time and resulted in large Fe influx. Four of these 16 cases ended with JET disruption.

5.2 HEAT LOADS ON THE LAUNCHER VIA IR CAMERA AND HOTSPOTS

Hotspots on a PFC magnetically connected to the LHCD launcher were observed before on JET [35,36,37] and on other machines [38,39,40,41]. In our study we refer to all areas seen on the IR cameras which are brighter than normal as hotspots. Clarification is needed, however, as LHCD can cause excessive heating of PFC either (i) by parasitically accelerating energetic electrons in SOL, which follow magnetic field lines and thus intercept on different in-vessel objects or (ii) by contributing to the power input and exhaust. In the former case hotspots are localised and magnetically connected to the LHCD launcher. In the second case brighter areas associated with either debris or surface layers can be seen usually in the divertor region during LHCD power phase, but not necessarily in regions on the same flux tubes as the launcher. The hotspots due to fast electrons are directly related to LH wave and SOL interaction and are thought to be more important regarding inner wall protection. While on the carbon-based machines allowable temperatures were much higher with ILW, surface temperatures above 950^{o}C were not allowed for Be PFC, and so special attention has been paid to the hotspots during LHCD in conditions with ILW. In general, hotspots due to LH were noticed during restart sessions; however, up to now no detrimental temperature increase has been observed for pulses up to 2.5MW of RF power and up to 5s duration.

When the LH power was increased above 2MW and with launcher placed between l_{pos}= –0.005m and +0.005m a hotspot in the middle of the ILA limiter can be clearly seen by the wide angle IR camera. The view of the camera and the approximate position of the hotspot, labelled as (1), are shown in figures 8 and 10. Its temperature increase was correlated with the LHCD power and it reached about 340^{o}C (figure 10) which is well below the safety limit of 950^{o}C for the limiter Be tiles. The large time constant characterizing the temperature increase/drop after LHCD switches on/off is an indication that a bulky limiter component has been warmed rather than a surface effect taking place. It was noted that the hotspot on ILA limiter moves downward with increasing equilibrium magnetic field, B_t, which proves that it is related to parasitical heating of a magnetically-connected PFC by an energetic electron beam confined within a magnetic flux tubes. In principle, the heat flux due to parasitically lost power in the SOL can be calculated from temperature measurements of the hotspots, [37]. This is however outside of the scope of this paper as the focus is mainly on safety issues related to the observed hotspots.

There is also an increase in temperature on the horizontal tiles on the bottom part of the outer divertor (labelled as (2) in figure 10), which is correlated with LHCD power. Preliminary investigation shows that no part of the LHCD launcher is magnetically connected to this area as shown in figure 8. It was concluded that the observed bright spots are actually debris (usually observed at the bottom of the divertor) and the increase of their temperature is due to the combination of plasma configuration with strike point at the corner used in LHCD pulses and the increase of the exhaust power. No relevant temperature measurement for these hotspots is available as the IR camera was not calibrated for W coated tiles and the existence of debris make the analysis and the interpretation of the results more difficult. Close examination of ICRH-only pulses

at similar corner configuration (see figure 3b and 4b) shows the same trends and the same relative increase in temperature with ICRH power. The conclusion is then that the observed bright areas are purely due to heating of debris and cannot be related to parasitic loss of LH power but are due to the combination of configuration change and exhaust power increase associated with LHCD.

In some cases the LHCD was misleadingly thought to cause hotspots. This is mostly seen of the divertor camera shown in bottom left corner of figure 8. More detailed investigation has shown that the fast increase and drop of the temperature with LHCD power observed in this case is an indication that probably a thin surface layer has been heated or other surface effect is taking place. Indeed, warming bulky PFC would result in much slower temperature variations as shown by time traces in figure 10b.

In order to validate the source of the observed hotspots a scan of the edge safety factor, q_{95}, was performed by varying B_t. There was no change in the positions of the bright spots on the divertor's horizontal tile with changing q_{95}, which is a clear indication that in this case debris are heated by the exhaust power. The suspected hotspot on the divertors' apron remains static during B_t ramp-up which proves that it is due to heating of a fixed layer on top of the divertor apron. A hotspot caused by energetic electrons parasitically accelerated by LH wave in SOL would move when changing q_{95} and magnetic field lines.

Images from an IR LHCD camera were used for the first time to assess the distribution of the heat on the launcher mouth during LHCD-only operation. The camera was not calibrated in time for JET campaigns and so absolute temperature measurements were not available. However, visual inspection and investigation of the heat load distributions and relative temperature changes could be done. The initial observations, figure 11, show that the grill is irregularly heated when launcher is moved closer to the plasma and LHCD power is applied. Provided that the launcher is melted predominantly on the left side and also at the top left corner [42] there is no clear indication that the hottest areas of the grill are the most damaged multijunctions.

Figure 11 also shows that the same sections of the grill are heated in these two JET pulses with similar plasma parameters and configurations but at different launcher positions. Placing the launcher closer to plasma further expands and makes the heated areas hotter (figure 11b). This effect is better pronounced at the top section of the grill (rows 1&2). Interestingly, the coupled RF power and the non-powered sections of the launcher seem to not have a strong impact on the pattern of the hot areas. Attention should be paid to the bottom-right hotspots (in the yellow box in the middle of rows 5&6) which are in the non-powered section of the grill. This indicates that harmful plasma-launcher interaction can occur in front of non-energised multijunctions as well. The investigation will further benefit from proper IR camera calibration and the analysis is planned to be completed by density, gas injection rates and LHCD power scans.

SUMMARY AND CONCLUSIONS

Overall, a relatively trouble-free operation of the LHCD system in the new ILW for up to 2.5MW

of coupled microwave power in L-mode plasma for time duration of up to 5s was achieved with no indication that the power cannot be increased further.

No significant impact on Be radiation with LHCD power was observed. Detailed analysis featuring assessment of W concentration by a dedicated code shows that LHCD contributes negligibly to W concentration increase. No W accumulation with LHCD-only heating is reported. LHCD coupling is not degraded with installation of ILW and is only slightly affected by the new operating conditions. Reflection coefficients were studied and coupling was optimised so that the system performance was brought back the levels achieved during carbon wall operation.

Improved Li-beam measurements allowed for SOL density measurements and first systematic study of the impact of LHCD on the SOL parameters. Gas injection rates, plasma density and configuration and launcher position were all scanned in optimising the coupling, while the relevant changes to the SOL parameters were documented by Li-beam measurements. The application of LHCD power leads to local increase in density in front of the powered sections of the grill. SOL density modifications have a typical 'hump' shape and scale with gas injection rate and LHCD power.

First observation of arcs in front of LH grill is reported. Arcs are not always stopped by existing protection and when not extinguished in time they seem to propagate along the row. A proposal to implement a new real-time protection acting only on the arcing klystrons is being considered as part of JET protection system and a project on its implementation has been started. It is believed that with this protection in place arcs can be stopped quickly enough to avoid the potentially dangerous consequences of damage to the launcher and plasma disruption.

Hotspots were observed but not found to be causing problems for powers up to 2.5MW and pulse durations of 5sec. The distribution of the heat loads across the front of the grill is not regular and further conclusions are pending calibration of the IR camera viewing the launcher.

ACKNOWLEDGEMENT

This work, supported by the European Communities under the contract of Association between EURATOM and CCFE, was carried out within the framework of the European Fusion Development Agreement. The views and opinions expressed herein do not necessarily reflect those of the European Commission. This work was also part-funded by the RCUK Energy Programme under grant EP/I501045 One of the authors (V. P.) acknowledges support by the Czech Science Foundation Project 205/10/2055, and of MSMT CR Grant Project ID LG11018. Authors would like to thank S. Devaux, G. Corrigan, P. da Silva Aresta Belo and D. Harting for help with IR camera data and EDGE2D code.

REFERENCES

[1]. G. Mathews et al, 2012, 20th International Conference on PSI, Eurogress, Aachen, Germany

[2]. J. Roth et al, 2008, Plasma Physics and Controlled Fusion **50** (2008) 103001

[3] S. Brezinsek et al, 2012, 39th European Physical Society Conference on Plasma Physics, Stockholm, Sweden, 2-6 July 2012

[4]. G. Hoang et al, 2009, Nuclear Fusion **49** (2009) 075001
[5]. G. Gormezano et al, 2007, Nuclear Fusion **47** (2007) S285
[6]. A. Tuccillo et al, 2005, Plasma Physics and Controlled Fusion **47** (2005) B363
[7]. R. Cesario et al, 2010, Nature Commun. (August 2010)
[8]. A. Ekedahl et al, 2010, Nuclear Fusion **50** (2010) 112002
[9]. B.J. Ding et al, 2011, Plasma Science and Technology, Vol.**13**, No.2, 153
[10]. M. Goniche et al, 2010, Plasma Physics and Controlled Fusion **52** (2010) 124031
[11]. K.K. Kirov et al, 2012, Plasma Physics and Controlled Fusion **54** (2012) 074003
[12]. K.K. Kirov et al, 2010, Nuclear Fusion **50** (2010) 075003
[13]. R. Parker et al, 2010, American Physical Society, 52nd Annual Meeting of the APS Division of Plasma Physics, November 8-12, 2010
[14]. V. Pericoli-Ridolfini et al, 2005, Nuclear Fusion **45** (2005) 1085
[15]. A. Tuccillo et al, 2012, 24th IAEA Fusion Energy Conference (FEC2012), San Diego, USA, 8-13 Oct. 2012
[16]. G.M. Wallace et al, 2011, Nuclear Fusion **51** (2011) 083032
[17]. G. Arnoux et al, 2012, 27th Symposium on Fusion Technology (SOFT), Liege, Belgium
[18]. K. Kirov et al, 2012, 39th European Physical Society Conference on Plasma Physics, Stockholm, Sweden, 2-6 July 2012
[19]. M. Pain et al, 1989, Proc. 13th Symposium on Fusion Engineering (Knoxville, TN)
[20]. M. Lenholmet al, 1995, Proc. 16th Symposium on Fusion Engineering (Champaign, IL)
[21]. K. Kirov et al, 2009, Plasma Physics and Controlled Fusion **51** (2009) 044003
[22]. C. Gormezano et al, 1993, "High Power Lower Hybrid Current Drive on JET: Results and Prospects," JET report, JET-P(93)65
[23]. T. Puetterich et al, 2008, Plasma Physics and Controlled Fusion **50** (2008) 085016
[24]. T. Puetterich et al, 2010, Nuclear Fusion **50** (2010) 025012
[25]. M-L. Mayoral et al, 2012, 24th IAEA Fusion Energy Conference (FEC2012), San Diego, USA, 8-13 Oct. 2012
[26]. V. Pericoli Ridolfini et al, 2004, Plasma Physics and Controlled Fusion **46** (2004) 349
[27]. A. Ekedahl et al, 2005, Nuclear Fusion **45** (2005) 351
[28]. A. Ekedahl et al, 2009, Plasma Physics and Controlled Fusion **51** (2009) 044001
[29]. M. Goniche et al, 2009, Plasma Physics and Controlled Fusion **51** (2009) 044002
[30]. M. Brix et al, 2010, Review of Scientific Instruments **81** (2010) 10D733
[31]. G. Matthews et al, 2002, Plasma Physics and Controlled Fusion **44** (2002) 689
[32]. R. Simonini et al, 1994, Contribution to Plasma Physics **34** p.368-73
[33]. V. Petrzilka et al, 2012, Plasma Physics and Controlled Fusion **54** (2012) 074005
[34]. V. Petrzilka et al, 2011, Plasma Physics and Controlled Fusion **53** (2011) 054016
[35]. K. Rantamaki et al, 2005, Plasma Physics and Controlled Fusion **47** (2005) 1101
[36]. M. Goniche et al, 1997, JET report, JET-R(97)14

[37]. P. Jacquet et al, 2011 Nuclar Fusion, **51** 103018
[38]. M. Goniche et al., 1998, Nuclear Fusion **38** (1998) 919
[39]. A. Ekedahl et al, 2009, Fusion Science and Technology **56**, 1150
[40]. J. Gunn et al., 2009, Jornal of Nuclear Materials **390–391**, p.904#
[41]. J. Mailloux et al., 1997, Jornal of Nuclear Materials **241-243**, p.745
[42]. K. Kirov et al, 2005, 16th Topical Conf. on RF Power in Plasmas, (Park City, UT), 11-13 Apr. 2005, AIP Conf. Proceedings **787**, eds. S Wukitch and P. Bonoli, p.315

(a) *(b)*

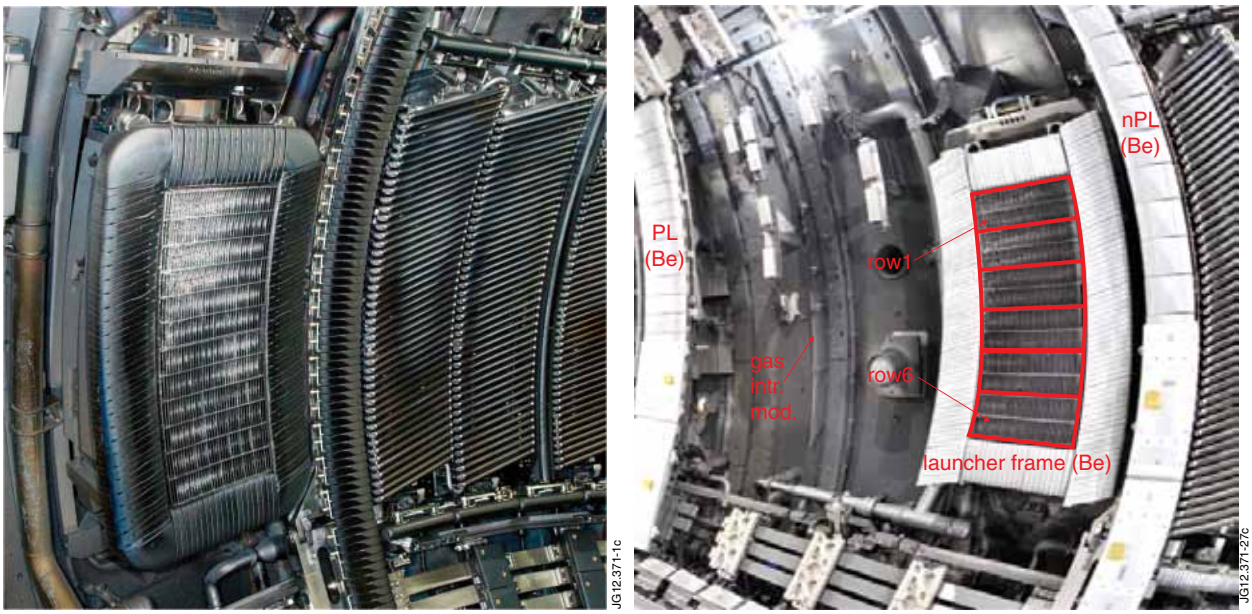

Figure 1: The old LHCD launcher as photographed from the left side in 2007 (a). A picture of the new launcher taken from right side in 2011 after its frame was replaced by Be one (b). Notations of rows 1 and 6 are provided as well as launcher frame, gas introduction module, poloidal limiter (PL) and narrow poloidal limiter (nPL) surrounding the launcher.

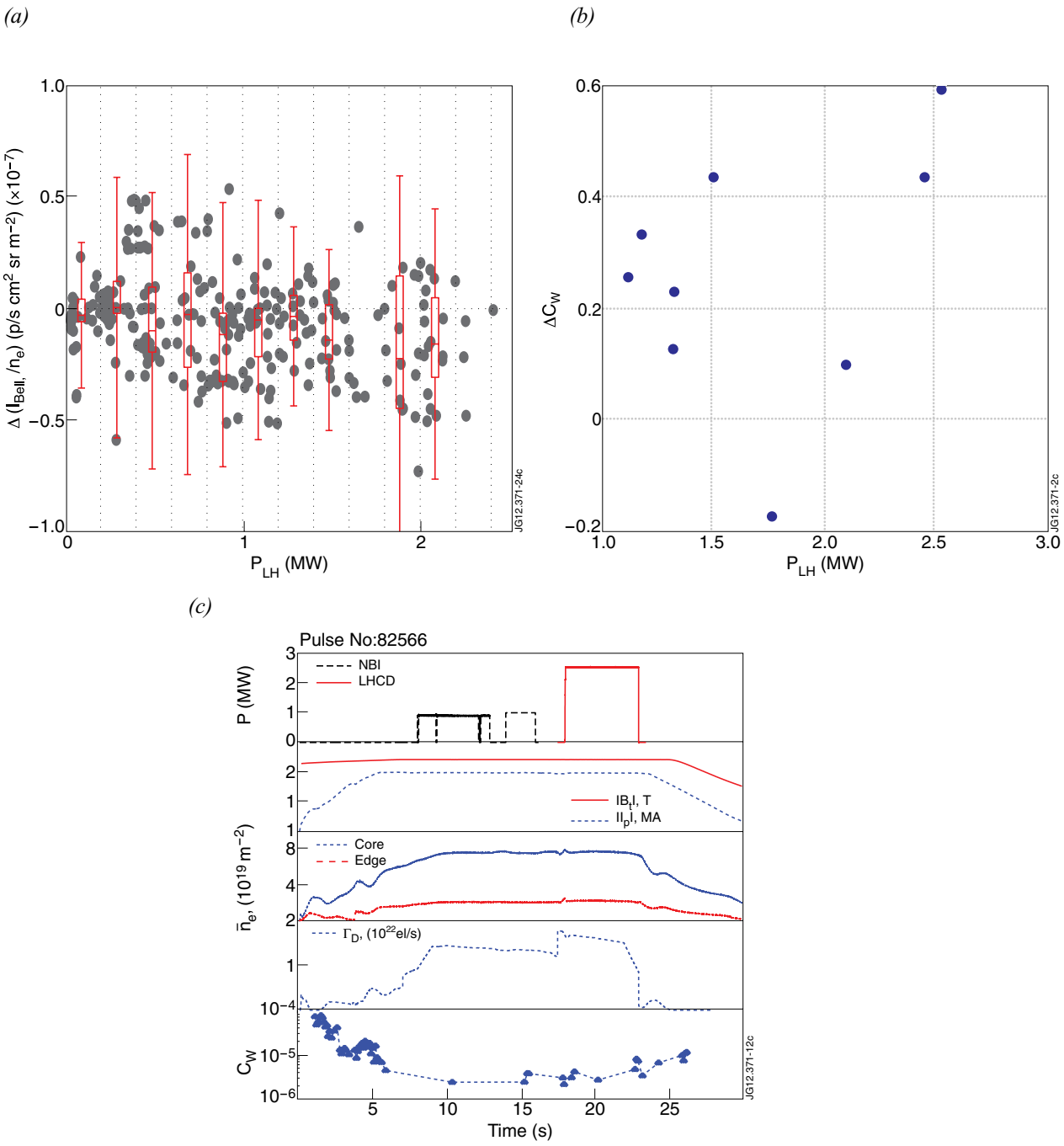

Figure 2: Increase of normalized emission from BeII (singly ionized Be, 527nm) is provided versus applied LHCD power (a). Data is also presented statistically as points are binned in 0.2MW intervals and boxplots represent lower, upper quartile and median while the whiskers show 98% of the observations for LHCD pulses. The increase in W concentration, ΔC_w, versus LHCD power is provided in (b). Data are taken from W analyser program which processes the data from available spectrometers and bolometers and uses plasma profiles from various diagnostics to assess the concentration of W, C_W. Time traces of a typical LHCD conditioning pulse with C_W from the W analyser program are shown in (c).

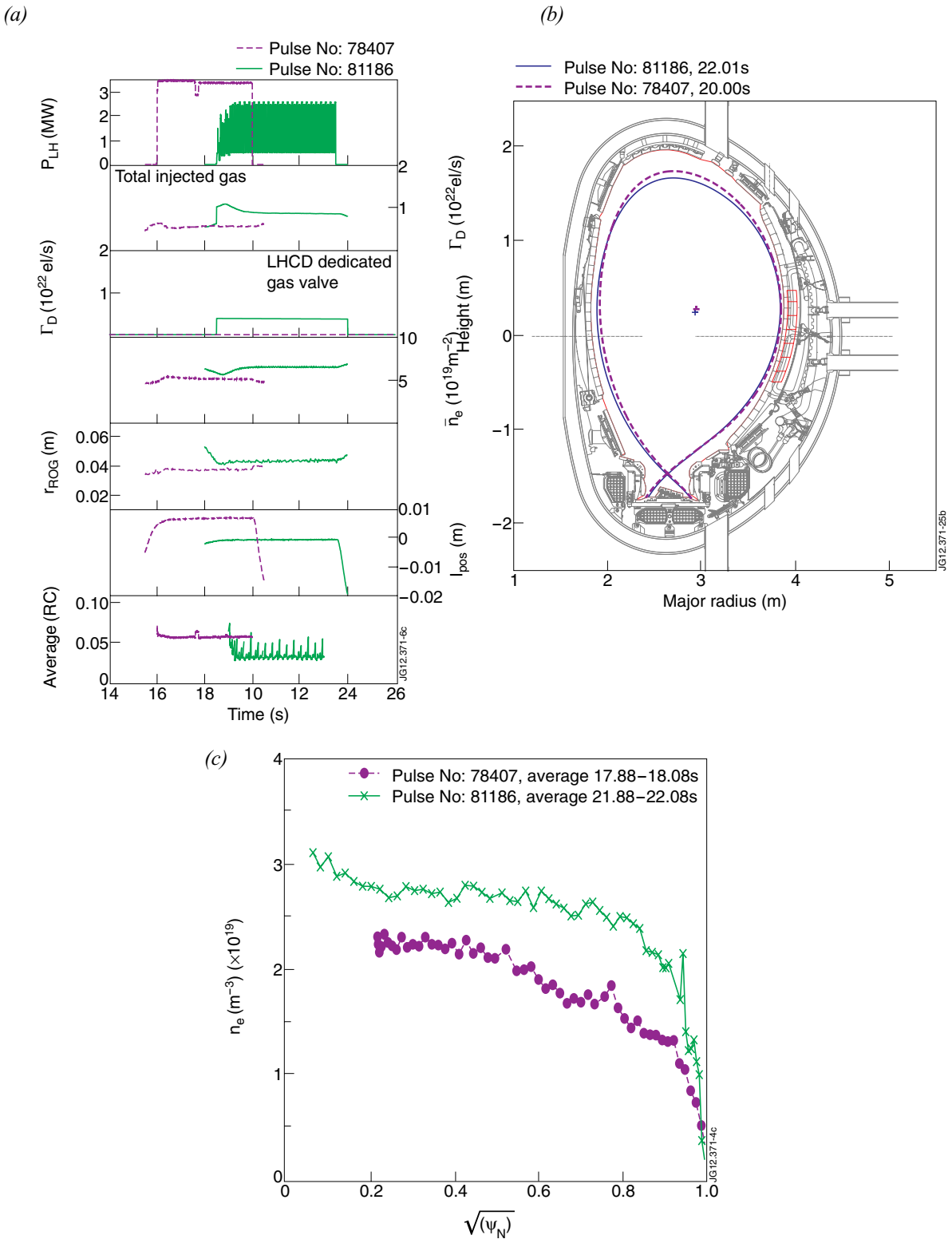

Figure 3: Comparison of LH conditioning pulses with CW and ILW. JET Pulse No: 78407 (2.2T/2MA with CW) and Pulse No: 81186 (2.2T/2MA with ILW) have somewhat different SOL and edge conditions expected to affect the LH coupling. In both cases however the average RCs are of the order of 0.05. Time traces of two pulses are shown in a), while the plasma shape is in b). Averaged density profiles from Thomson Scattering (TS) diagnostic are provided in c).

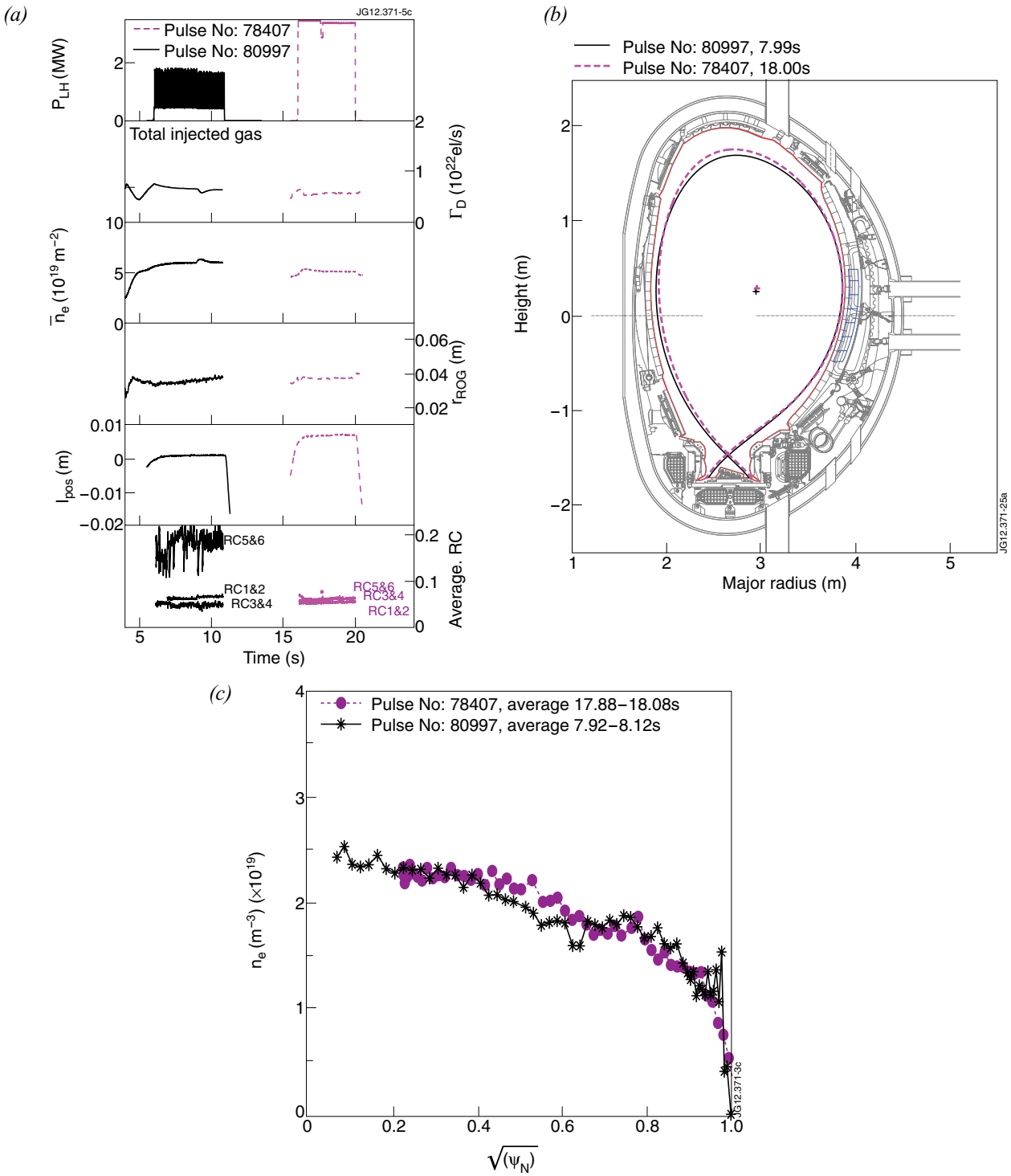

Figure 4: LHCD coupling with C wall and ILW conditions. Time traces of two similar pulses with no gas from dedicated gas injection valve, Pulse No: 78407 (2.2T/2MA, magenta) and Pulse No: 80997 (2.28T/2MA, black), are compared in a). From top to bottom shown are the LHCD power, total gas injection rate, line integrated density, plasma-limiter clearance, r_{ROG}, limiter launcher distance, l_{pos}, and averaged RCs on rows 1&2, 3&4, and 5&6 are shown. Plasma shapes for the two cases are given in b), while density profiles are provided in c).

(a) *(b)*

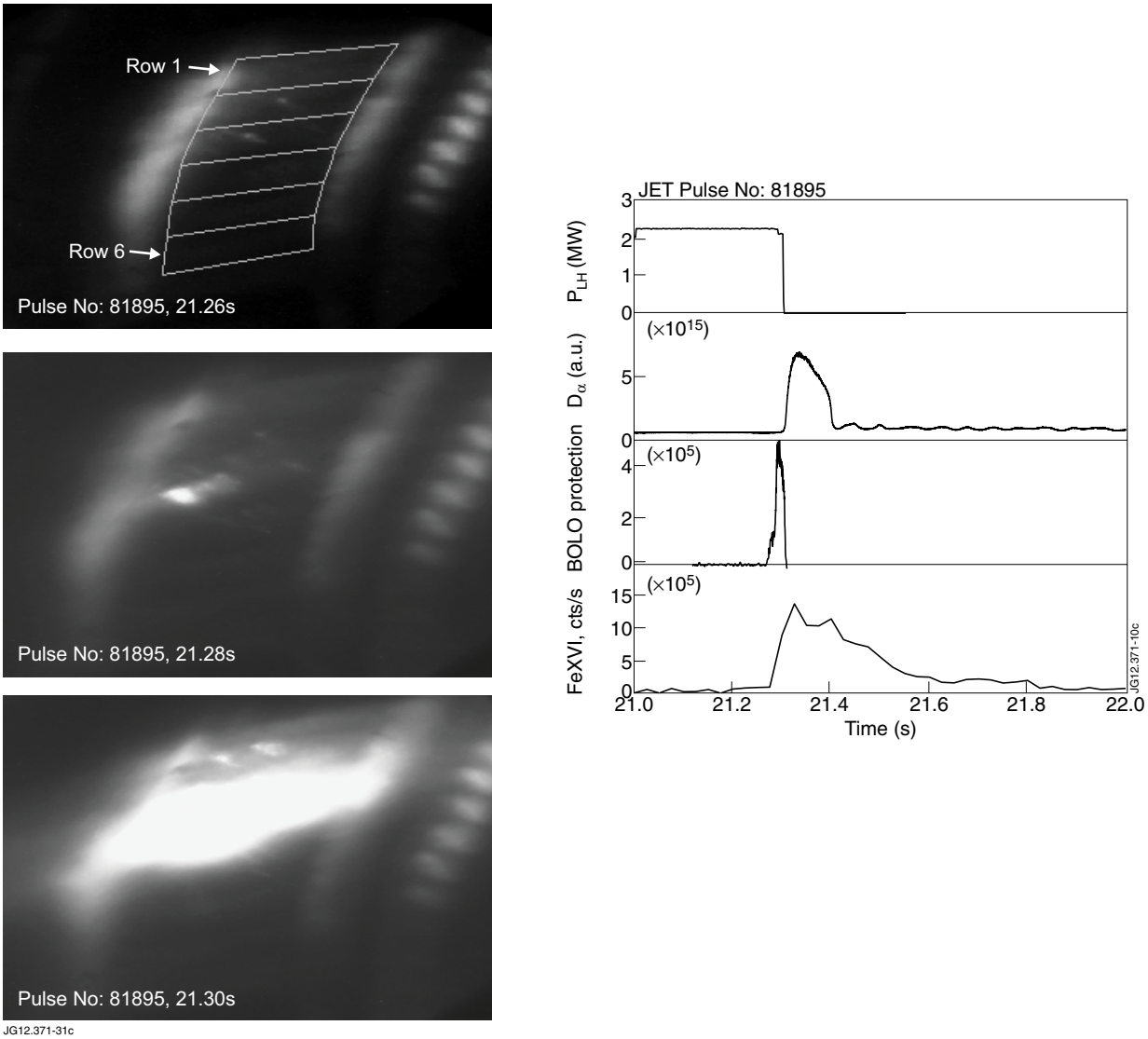

Figure 5: (a) LHCD RCs on rows 1 to 6 for four values of gas puff rate (provided in the legend) from dedicated gas injection module. The RCs when klystrons are tripping are shown by symbols, black + for Pulse No: 61302, row1 and green dots for Pulse No: 61303, rows1, 2, 5, and 6. (b) Time traces of the gas injection, total and from dedicated valve, electron density, line integrated, central and at the pedestal (β_N=0.9), and SOL density at midplane position of PL, R_{mid}=3.889m, by Li-beam.

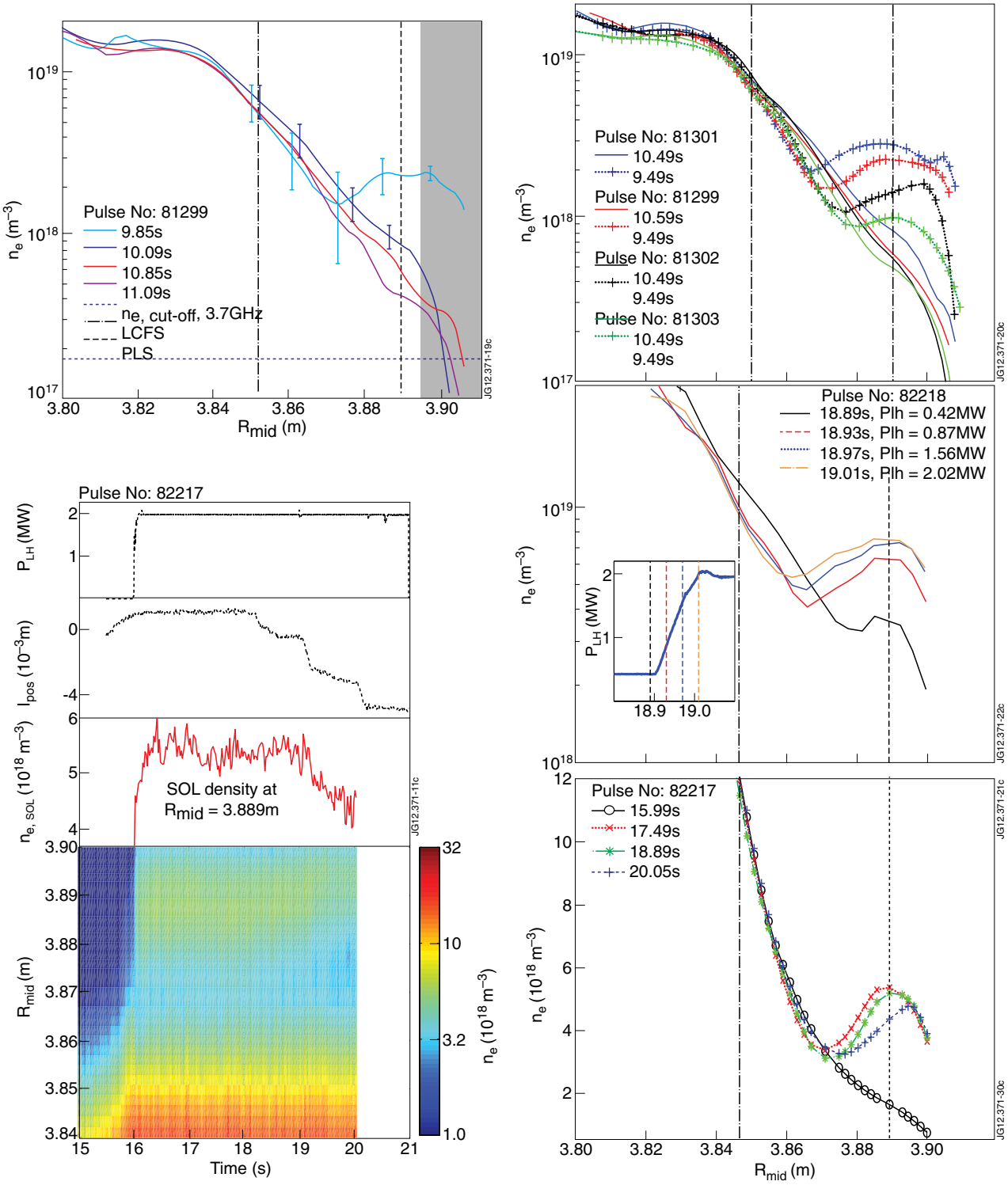

Figure 6: Li beam profiles for 2.7T/2.45MA JET Pulse N o: 81299 with gas injection rate from dedicated gas valve of 4×10^{21} el/s and rows 3&4 magnetically connected to the diagnostic (a). Time traces of the power waveforms are provided in figure 5(a) as well. Private SOL region of Li-beam diagnostic where measured density is not directly affected by LHCD power is shadowed in (a) while separatrix (dash-dotted line) and poloidal limiter (dashed line) projections at the midplane radius are shown for all radial profiles. SOL profiles with ('+' symbols) and without (solid lines) LHCD power for different gas injection rates, see also figure 5(b), are provided in (b). The impact of the microwave power can be seen in (c) where four SOL density profiles during LHCD power ramp-up (inset graph) are shown. Effect of the launcher position is shown in (d) where 2MW of LH power was applied in Pulse No: 82217 and launcher retracted back as shown by l_{pos} trends. The density at the limiter (R_{mid} =3.889m) and colorplots versus time and R_{mid} are provided as well. SOL profiles at 15.99s (no LH power), 17.49s (l_{pos}~+0.001m), 18.89s (l_{pos}~0.000m) and 20.05s (l_{pos}~–0.003m) are given in (e).

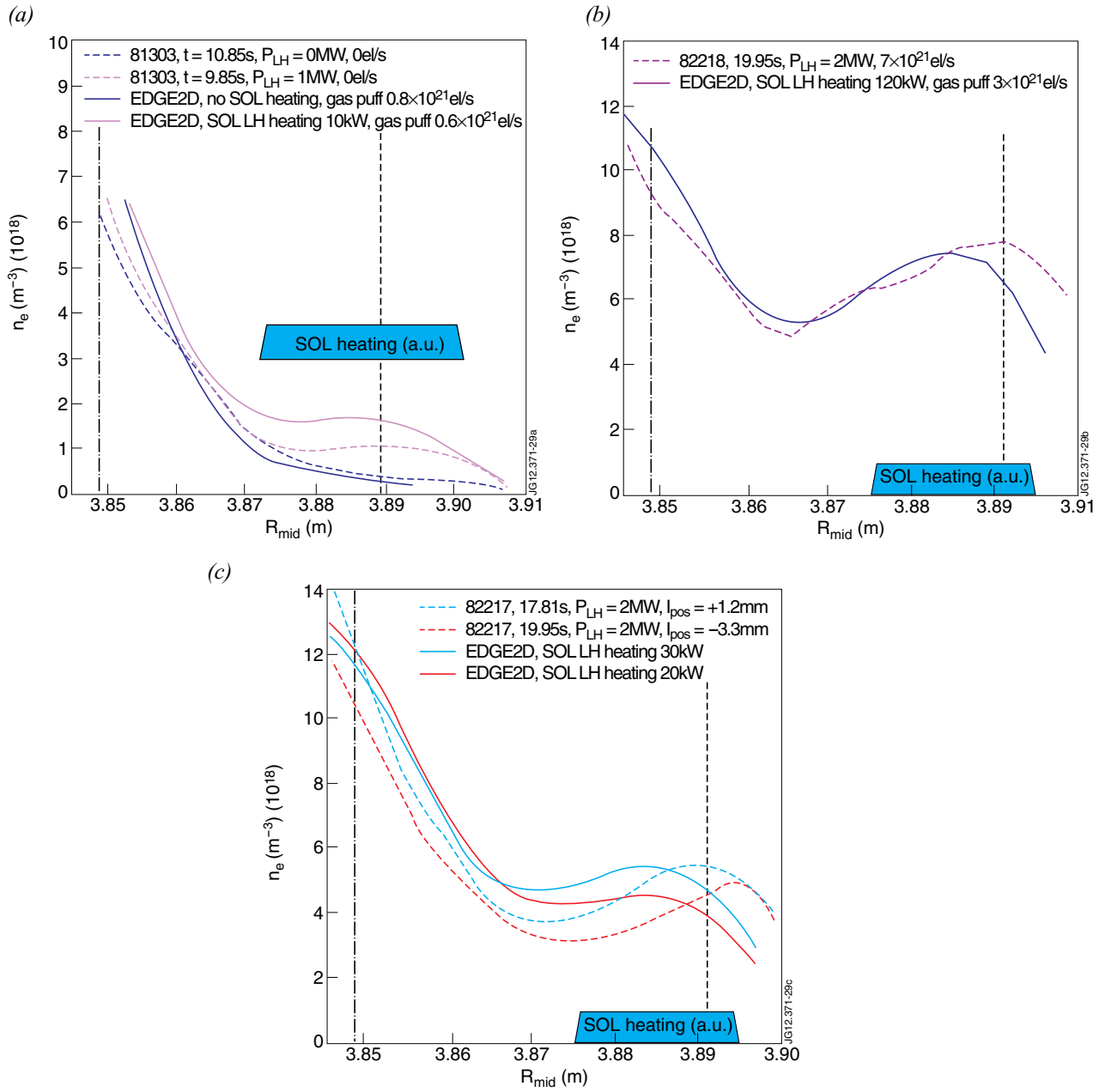

Figure 7: Measured Li-beam SOL density profiles (thick dashed lines) without (blue) and with (magenta) LH power for Pulse No: 81303 (a). EDGE2D modelling results are provided (thin solid lines) assuming zero (blue) or 30kW (magenta) of parasitic LH heating in a.u. between R_{mid} = 3.87m and R_{mid} = 3.90m (cyan rectangle). LHCD power and the gas injection rates – as used in the model and from dedicated valve – are given in the legend. Experimental data (thick dashed line) and EDGE2D (thin solid line) simulations for Pulse No: 82218 with gas injection rate from dedicated vale of 7×10^{21} el/s are shown in (b). Li-beam data and EDGE2D simulations for Pulse No: 82217 when 2MW of LH power was applied while launcher placed at different positions are shown in (c).

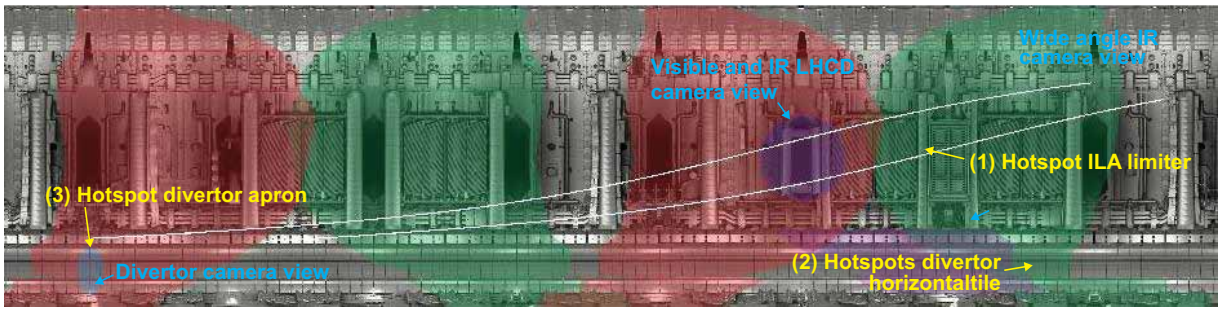

Figure 8: A sketch of JET cameras view with two magnetic field lines covering the front of the LHCD launcher for a typical 2.4T/2MA JET Pulse No: 81382, 18.08s. Hotspots positions are provided by yellow arrows and labels, while cameras' views are indicated by cyan arrows and labels.

(a)

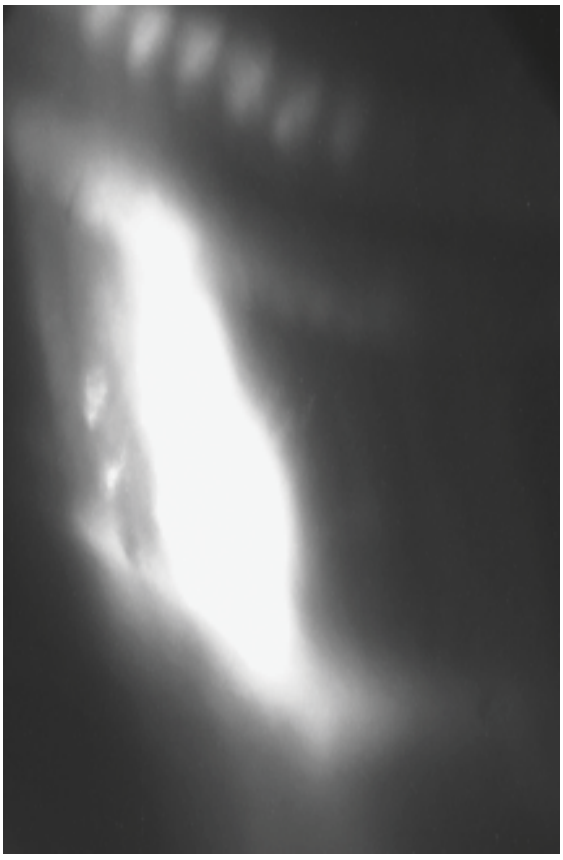

(b)

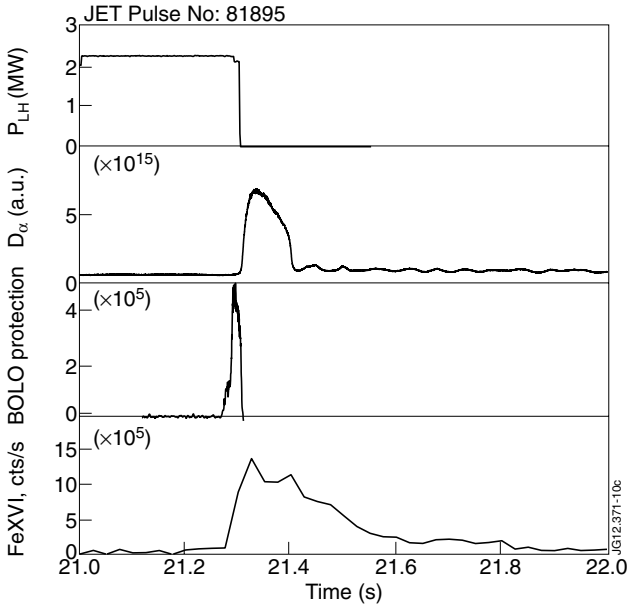

Figure 9: Arc seen on the visible LHCD camera in three consecutive frames, #81895, 21.26s, 21.28s and 21.30s, showing how an arc develops into a flare in front of rows 2&3. On the right, the time traces of the LHCD power, D_α signal as well as the signals from bolometer and FeXVI line used in arc protection based on impurity radiation are shown.

(a) (b)

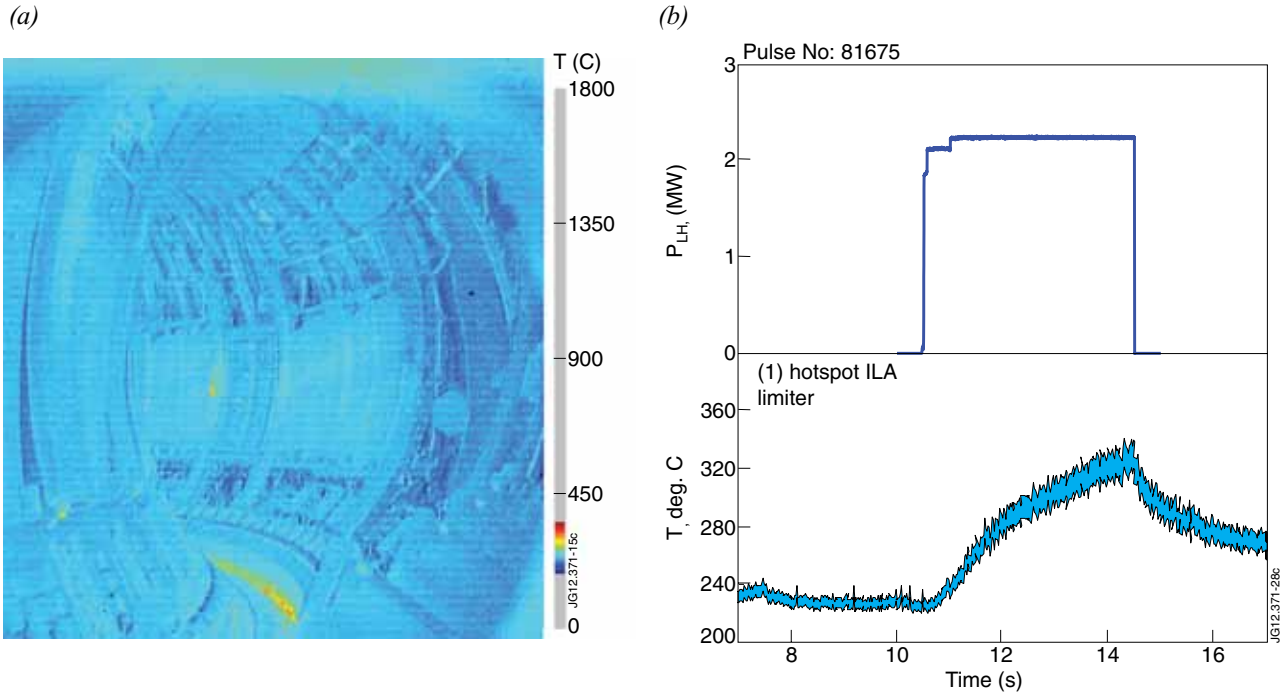

Figure 10: IR image of the plasma interior during a 2.3MW LHCD JET Pulse No: 81675, 14.42s (a) and time traces of the LHCD power and temperature range of hotspot (1) on ILA limiter (b). No relevant temperature measurement for hotspots (2) is available as the IR camera was not calibrated for W coated tiles and the debris make the analysis more complicated.

(a) (b)

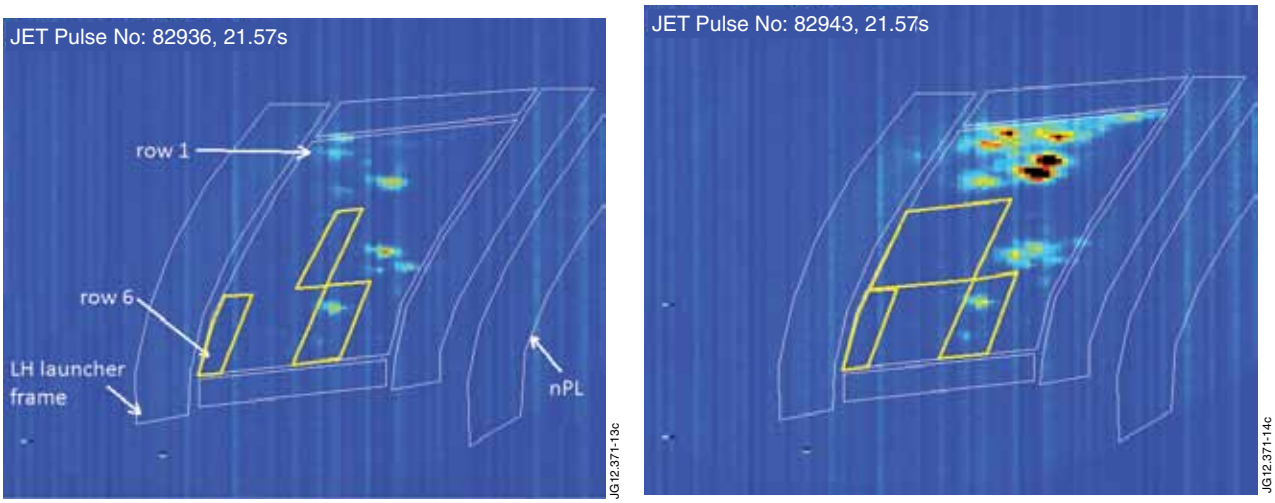

Figure 11: IR LHCD camera images of the launcher showing hottest areas of the grill for a) 2.4T/2MA JET Pulse No: 82936, 21.57s with P_{LH}~1.6MW from 18s to 23s with 20 klystrons all pulsing with ~85kW of RF power and l_{pos}~0.008m; and b) 2.4T/2MA JET Pulse No: 82943, 21.57s with P_{LH}~1.4MW from 18s to 23s with 17 klystrons all pulsing with ~85kW of RF power and l_{pos}~0.013m. Image is colour coded so that the temperature increase is indicated by gradually changing colour sequence blue – cyan – green - yellow – red - black. The LH launcher frame, nPL and approximate positions of rows 1 and 6 are shown in white. The approximate positions of the non energised sections of the grill are show in yellow, while the rest of the klystrons are powered with ~85kW.